Desalination and Water Treatment
www.deswater.com

doi: 10.5004/dwt.2023.29222

283 (2023) 259–273
January

Electrochemical properties of Ti/Sb/SnO$_2$-SiO$_2$ anode for electrocatalytic oxidation of Acid Red 18

Yanfang Song, Jiaman Liu, Jiping Jia, Honghua Ge*, Xinjing Meng*, Yuzeng Zhao*

Shanghai Engineering Research Center of Energy-Saving in Heat Exchange Systems, Shanghai Key Laboratory of Materials Protection and Advanced Materials in Electric Power, Shanghai University of Electric Power, Shanghai 200090, China, emails: gehonghua@shiep.edu.cn (H.H. Ge), mengxinjing@shiep.edu.cn (X.J. Meng), zhaoyuzeng@shiep.edu.cn (Y.Z. Zhao), yanfang_song16@163.com (Y.F. Song), 17351873398@163.com (J.M. Liu), m17301781770@163.com (J.J. Ping)

Received 27 April 2022; Accepted 11 December 2022

ABSTRACT

In this paper, Ti/Sb/SnO$_2$-SiO$_2$ electrodes were prepared by adding SiO$_2$ nanoparticles with high thermal stability as barrier substance on the Ti/Sb/SnO$_2$ electrodes, and the electrocatalytic performance of the Ti/Sb/SnO$_2$-SiO$_2$ electrode and degradation effect on Acid Red 18 (AR 18) was examined. The results showed that coating with SiO$_2$ nanoparticles had better compactness and smaller *crystal* grains than that without SiO$_2$, because the addition of SiO$_2$ nanoparticles hindered the growth of SnO$_2$ grains. The addition of SiO$_2$ nanoparticles also increased the oxygen vacancies in the coating, raising the active oxygen content, which can improve the generation capacity of $^{\bullet}$OH. Compared with Ti/Sb/SnO$_2$ electrode, the Ti/Sb/SnO$_2$-SiO$_2$ electrode had a larger specific surface area and oxygen evolution overpotential, which can inhibit the occurrence of side reactions of oxygen evolution, improving the degradation efficiency of AR 18. The degradation process conformed to first-order kinetics. Meanwhile, the degradation intermediate product was inferred according to the results of the three-dimensional fluorescence test. In addition, the addition of SiO$_2$ nanoparticles improved current efficiency and reduced energy consumption, significantly strengthening electrode stability.

Keywords: Electrocatalytic oxidation; SiO$_2$ nanoparticles; Ti/Sb/SnO$_2$-SiO$_2$ electrode; Electrochemical activity; Hydroxyl radicals

---

1. Introduction

Dyes are widely used in the textile, paper, leather, plastic and food industries [1–4]. With the rapid development of light industry, the discharge of dye wastewater is gradually increasing. Therefore, dye wastewater has become one of the important research objects in wastewater treatment. The pollution load of dye wastewater is usually large, which will cause a decrease of dissolved oxygen in the water and have an adverse effect on the organism. Discharging dye wastewater directly into the water without treatment will seriously affect the balance of the water environment and destroy the ecological environment [5,6]. Due to the aromatic ring in the structure of azo dyes, they can cause great harm to the human body [4,7]. After conventional physicochemical and biochemical methods have been used to treat this wastewater, there are still large amounts of non-degradable substances and colours [6], resulting in failure to meet the allowable emission standards. Faced with these problems, researchers began to study new processing technologies such as electrocatalysis [8], photocatalysis [9,10], the electro-Fenton process [3], synergy of the above technologies, and so on [11,12], which are promising advanced oxidation technologies for the treatment of organic pollutants [13]. Because of their efficient oxidizing ability and easy operation advantages, extensive research has been conducted in recent years.

---

* Corresponding authors.

Electrocatalytic oxidation technology produces a kind of active oxygen with strong oxidation ability on the anode surface, such as hydroxyl radicals (•OH). OH can attack and destroy the structure of dyes and can ultimately cause organic pollutants to be effectively mineralized [14,15]. Titanium-based tin antimony electrode (Ti/Sb/SnO_2) has low cost and high oxygen evolution potential and has thus attracted attention. However, it still has problems of insufficient stability and low wastewater treatment efficiency, which are usually solved by doping with metal particles [16–19]. At present, carbon nanotubes and TiO_2 nanotubes have been widely used in the field of electrocatalysis [20–26]. The SiO_2 nanoparticles have the characteristics of small particle size, large specific surface area, and good thermal stability and are thus widely used in corrosion-resistant coatings [27–29]. These characteristics of SiO_2 nanoparticles may have a good promotion effect on the performance of anode materials. Therefore, SiO_2 nanoparticles were applied to prepare Ti/Sb/SnO_2-SiO_2 anode in this paper. The influence of SiO_2 nanoparticles on the electrochemical characteristics of the Ti/Sb/SnO_2-SiO_2 anode and the electrocatalytic oxidation performance of this electrode on the persistent refractory organic pollutants Acid Red 18 (AR 18) were investigated.

2. Experimental materials and methods

2.1. Experimental materials and media

In the experiment, pure titanium TA1 was used as the substrate of the anode material, components of which are O (≤0.15%), C (0.05%), Fe (0.15%), N (0.03%), H (0.012%), Si (0.1%), other (0.05%), and Ti (margin). The chemical reagents used in the experiment were all of analytical grade. Deionized water was used for solution preparation.

2.2. Electrode preparation

First, a mixed isopropanol solution of $SnCl_2\cdot 2H_2O$, Sb_2O_3, and 3 g/L SiO_2 nanoparticles was prepared as the coating solution after mixing evenly. Second, a brush was used to uniformly coat the coating solution on degreased and acid-etched the titanium surface. The detailed steps in accordance with our previous preparation method [30].

2.3. Electrode surface characterization

The surface morphology and the crystal structure of the coatings on titanium were characterized by scanning electron microscope (SEM) and X-ray diffractometer (XRD). The chemical state of the electrode surface was detected by X-ray photoelectron spectroscopy (XPS). The coating thickness was measured with a coating thickness gauge.

2.4. Electrochemical test

The electrochemical test was carried out in 0.5 mol/L H_2SO_4 solution. The scanning speed of both linear scanning voltammetry (LSV) and cyclic voltammetry (CV) was 50 mV/s. The frequency range of electrochemical impedance spectroscopy was from 100 kHz to 0.01 Hz.

2.5. Electrocatalytic oxidation

The electrocatalytic oxidation experiment used a 0.4 mol/L Na_2SO_4 solution containing a certain AR 18 concentration. The current density of the electrocatalytic oxidation experiment was controlled to 100 mA/cm^2 by using a regulated power supply. The chemical oxygen demand (COD) test adopted a multi-parameter water quality analyser. The absorbance of electrolyte is measured by an UV-Vis spectrophotometer. A fluorescence spectrophotometer was used to measure the three-dimensional fluorescence spectrum and hydroxyl radical intensity of fluorescence. The scanning range of the excitation wavelength was 220–500 nm, and the emission wavelength was 220–500 nm. In the electrocatalytic oxidation process, phthalic acid was used as a probe; it reacted with •OH to produce stable 2-hydroxyterephthalic acid. The intensity of 2-hydroxyterephthalic acid was measured by three-dimensional fluorescence indirectly to indicate the intensity of OH.

3. Results and discussion

3.1. Morphology and crystal structure of the electrode

Fig. 1a and b show the surface morphology of the two coatings. Fig. 1c and d show the atomic percentage and element distribution of the two coatings. In Fig. 1a there are large, deep cracks on the surface of the Ti/Sb/SnO_2 coatings. The cracks on the surface of the Ti/Sb/SnO_2-SiO_2 electrode are obviously reduced and relatively uniform, which indicates that the addition of SiO_2 nanoparticles can effectively improve the structure of the coating, thereby preventing impact of the electrolyte on the titanium substrate [31,32]. The energy-dispersive X-ray spectroscopy (EDS) analysis results in Fig. 1c and d shows that the main elements in the coating, Sn, O, Sb, and Si, are evenly distributed on the electrode surface. Compared with Fig. 1c, in Fig. 1d the same uniform distribution of Si elements can be clearly observed, indicating that SiO_2 nanoparticles were successfully added on the surface of the Ti/Sb/SnO_2-SiO_2 electrode.

XRD was used to analyse the crystal structure of the coating, as shown in Fig. 2. No diffraction peak of Sb is seen in Fig. 2, which may indicate that Sb can enter the crystal lattice of SnO_2 by substitution. Compared with Ti/Sb/SnO_2, the peak of Ti/Sb/SnO_2-SiO_2 has a larger half-width, which shows that the SnO_2 crystal grains in the Ti/Sb/SnO_2-SiO_2 electrode coating are smaller. Thereby, more active sites can be provided, which can improve the electrocatalytic oxidation ability of the electrode. The thermal stability of SiO_2 nanoparticles is the main reason for the smaller grain size of SnO_2. SiO_2 nanoparticles act as a physical barrier during SnO_2 crystal formation, reducing the chance of collisions between SnO_2 grains, resulting in smaller grains. In addition, the coating thickness of Ti/Sb/SnO_2 and Ti/Sb/SnO_2-SiO_2 electrodes measured by the coating thickness gauge is about 80 nm. But the diffraction peak of Ti becomes weaker after adding SiO_2 nanoparticles, indicating that Ti/Sb/SnO_2-SiO_2 coating has better coverage than Ti/Sb/SnO_2 coating. This can help to improve the electrochemical activity and stability of the electrode [33,34].

The spectra of O 1s in the two coatings were analysed by XPS. It can be seen from Fig. 3 that two XPS spectra of

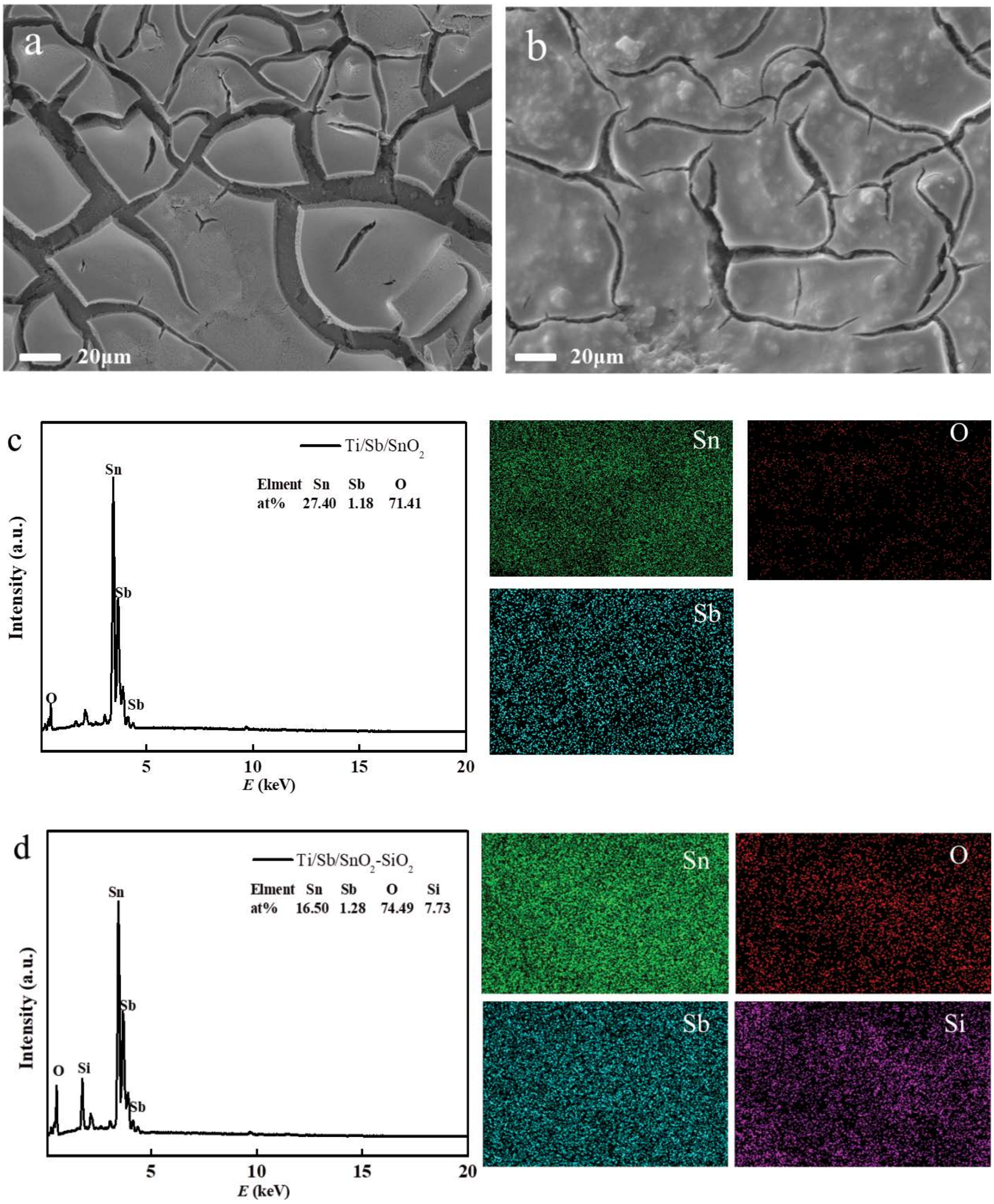

Fig. 1. SEM image and EDS image of the two electrodes: (a,c) Ti/Sb/SnO_2-SiO_2 and (b,d) Ti/Sb/SnO_2-SiO_2

O 1s bands located at around 530.7 and 532.6 eV were obtained after deconvolution. The low binding energy peak at 530.7 eV corresponds to the oxygen atom (O_{lat}) that forms the bond with the metal atom, while the high binding energy peak at 532.6 eV corresponds to the hydroxyl oxygen atoms (O_{ads}) adsorbed on the electrode surface [34]. The content of O_{lat} and O_{ads} in the coating can be calculated based on the corresponding peak area. The results are listed in Table 1. The O_{ads} content of Ti/Sb/SnO_2-SiO_2 coating (36.59%) is significantly higher than that of Ti/Sb/SnO_2 coating (22.82%). The electrode with higher O_{ads} content has better hydroxyl radical generation ability [35], which can promote the degradation of pollutants, indicating that the electrocatalytic oxidation ability of the electrode can be improved by adding SiO_2 nanoparticles. The Sb $3d_{3/2}$ orbital was divided into two peaks Sb^{3+} and Sb^{5+}, and the content of Sb^{3+} in the coating can be calculated based on the corresponding peak area. It was found that the valence state of Sb in the coating changed greatly before and after adding SiO_2 nanoparticles (Sb^{3+} content increased from 38.68% to 67.40%, Table 1). The addition of a trivalent cation such as Sb^{3+} to SnO_2 increased the number of oxygen vacancies [36]. Therefore, the addition of SiO_2 nanoparticles made the valence state of Sb atoms on the coating surface tend to be trivalent, so that the coating surface had more oxygen vacancies.

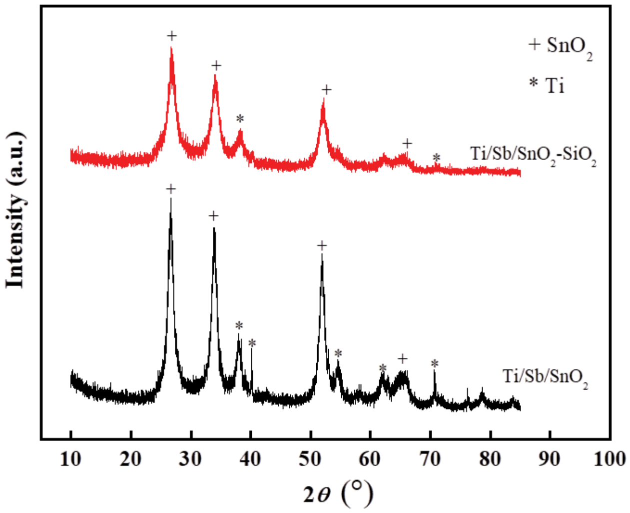

Fig. 2. XRD patterns of the two electrodes.

3.2. Electrochemical test

Fig. 4 shows the LSV curves of the two electrodes. The oxygen evolution potentials of the Ti/Sb/SnO_2 and Ti/Sb/SnO_2-SiO_2 electrodes are 2.06 and 2.20 V, respectively. The Ti/Sb/SnO_2-SiO_2 electrode has a higher oxygen evolution potential. The increase in oxygen evolution potential is related to the low lattice oxygen content and higher crystallinity of the coating [34,35,37], indicating that the electrode can better inhibit the side reaction during electrochemical oxidation after adding SiO_2 nanoparticles, which can improve current efficiency.

In order to explore the effect of adding SiO_2 nanoparticles on the electrocatalytic activity of the electrode, the

Table 1
XPS parameters of the two electrodes

Electrode	Binding energy (eV)			Atom ratio	
	Sb $3d_{3/2}$	O_{lat}	O_{ads}	Sb^{3+} content (%)	O_{ads} content (%)
Ti/Sb/SnO_2	540.8	530.6	532.3	38.68	22.82
Ti/Sb/SnO_2-SiO_2	540.8	530.5	531.8	67.40	36.59

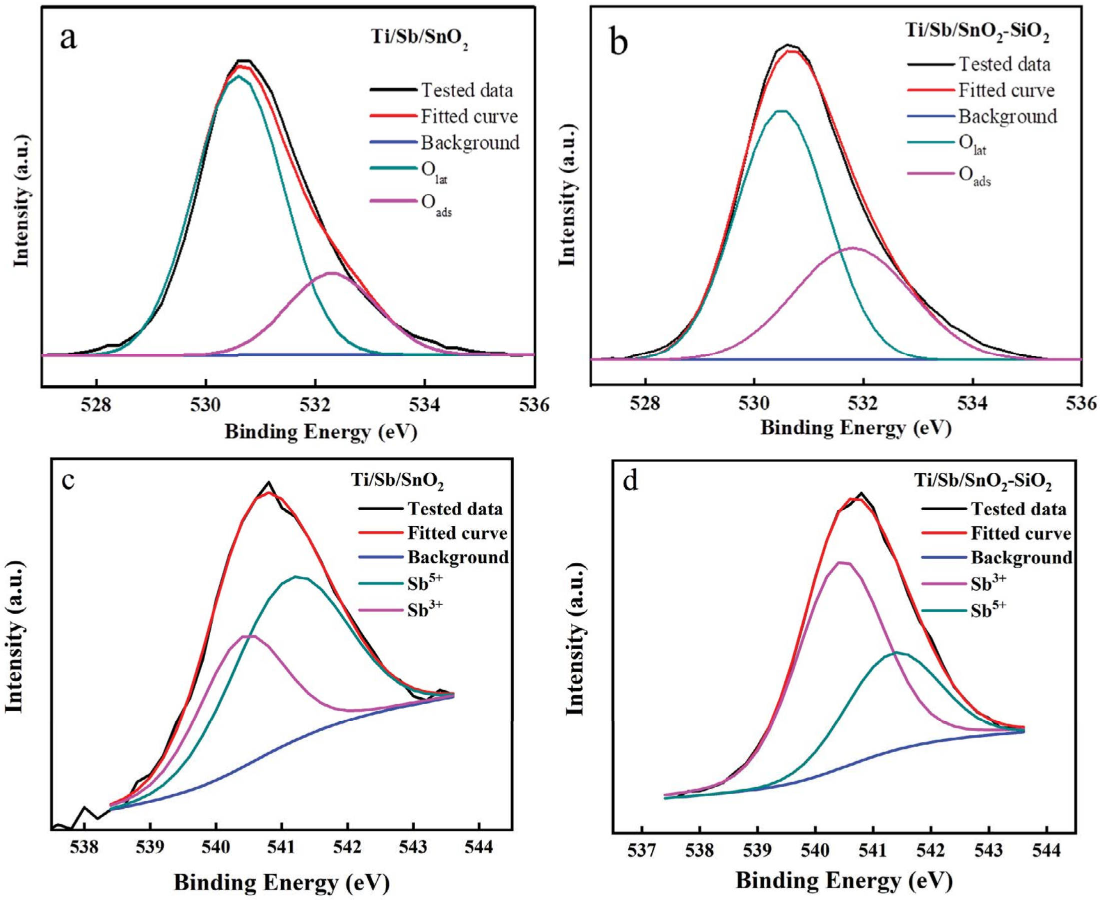

Fig. 3. XPS spectra analysis of O 1s and Sb $3d_{3/2}$ on the two electrodes.

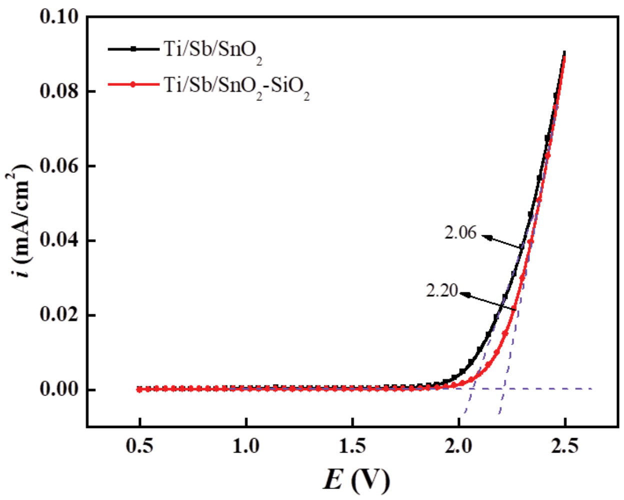

Fig. 4. LSV curves of the two electrodes.

surface roughness coefficients and volt-ampere charges of the two electrodes were compared by CV [38]. The roughness coefficient reflects the actual specific surface area of the electrode, which can be calculated by comparing the electrochemical double layer capacitance of the electrode surface and the smooth SnO_2 surface [39]. Fig. 5a and b show the CV curves of the Ti/Sb/SnO_2 and Ti/Sb/SnO_2-SiO_2 electrodes at different scan rates, respectively. According to the CVs of Fig. 5a and b, the relationship between the current density i and scan rate v is obtained, as shown in Fig. 5c, and the linear relationship illustrates the non-Faraday characteristics of the current in this region [34]. Using Eq. (1), the electric double layer capacitance can be calculated:

$$i_c = v \cdot C_{\mathrm{dl}} \tag{1}$$

where i_c, v, and C_{dl} are the non-Faraday capacitance current, scan rate, and electric double layer capacitance, respectively. The calculated electric double layer capacitances of the Ti/Sb/SnO_2 and Ti/Sb/SnO_2-SiO_2 electrodes are 4.83 and 14.03 μF/cm^2, respectively. The roughness coefficient (r) can be calculated according to Eq. (2) [34]:

$$r = \frac{C_{\mathrm{dl}}}{C_S} \tag{2}$$

where C_s is the electric double-layer capacitor on the smooth SnO_2 surface, generally $C_s = 8$ μF/cm^2 [39].

The calculated roughness coefficient of the Ti/Sb/SnO_2-SiO_2 electrode is 2.9 times that of the Ti/Sb/SnO_2 electrode, which proves that the addition of SiO_2 nanoparticles can significantly improve the surface roughness of the electrode, enhancing the electrocatalytic activity of the electrode beneficially.

Fig. 5d shows the CV curves of the two electrodes at 50 mV/s. It can be found that the area enclosed by the CV curve of the Ti/Sb/SnO_2-SiO_2 electrode is significantly larger than that of the Ti/Sb/SnO_2 electrode. This shows that the volt-ampere charge (q*) of Ti/Sb/SnO_2-SiO_2 is larger, meaning that the electrochemically active area is larger. By calculating the volt-ampere charge, the electrochemically active area of the electrode can be further compared. Fig. 5e and f show the relationship between the volt-ampere charges of the two electrodes and the scan rate. The total volt-ampere charge (q_T*) is related to the total electrochemically active area of the coating, which can be obtained by the relationship between q* in Eq. (3) and the scanning rate:

$$\left(q^*\right)^{-1} = \left(q_T^*\right)^{-1} + k_1 v^{1/2} \tag{3}$$

where k_1 is the slope of the fitted curve.

The total volt-ampere charge can be divided into external volt-ampere charges and internal volt-ampere charges. The external volt-ampere charge (q_0*) is related to the outer active area where the oxidation reaction occurs and can be obtained by Eq. (4):

$$q^* = q_o^* + k_2 v^{-1/2} \tag{4}$$

where k_2 is the slope of the fitted curve.

In the electrocatalytic oxidation process, the electrolyte can easily diffuse into the coating through the surface of the electrode [33]. However, due to the denser coating of Ti/Sb/SnO_2-SiO_2, the electrolyte diffusion rate is relatively slow. The internal volt-ampere charge (q_i*) can be calculated by Eq. (5):

$$q_i^* = q_T^* - q_o^* \tag{5}$$

The electrochemical porosity (p) is the ratio between the internal volt-ampere charge and the total charge, as shown in Eq. (6):

$$p = \frac{q_i^*}{q_T^*} \tag{6}$$

The results of volt-ampere charges and electrochemical porosity of the Ti/Sb/SnO_2 and Ti/Sb/SnO_2-SiO_2 electrodes are shown in Table 2. The results show that the Ti/Sb/SnO_2-SiO_2 electrode with SiO_2 nanoparticles has a higher porosity and volt-ampere charge, indicating that the addition of SiO_2 nanoparticles can increase the effective electrochemical surface area of the electrode, which can provide more active sites for the electrode reaction [33].

Fig. 6 shows the electrochemical impedance spectroscopy of the two electrodes. The electrochemical impedance spectroscopy of the two electrodes only shows capacitive reactance arcs, illustrating that the charge transfer plays a major role in the electrode process. The equivalent circuit in Fig. 7 is used to fit the electrochemical impedance spectrum, where R_s is the solution resistance, R_f is the resistance of the electrode surface coating and C_f is the capacitance of the electrode surface coating, C_{dl} is the double layer capacitance, and R_{ct} is the charge transfer resistance. Table 3 shows the fitting results. The smaller the R_{ct} value, the faster the electrochemical reaction rate. As can be seen from Table 3, the R_{ct} of the electrode is significantly reduced

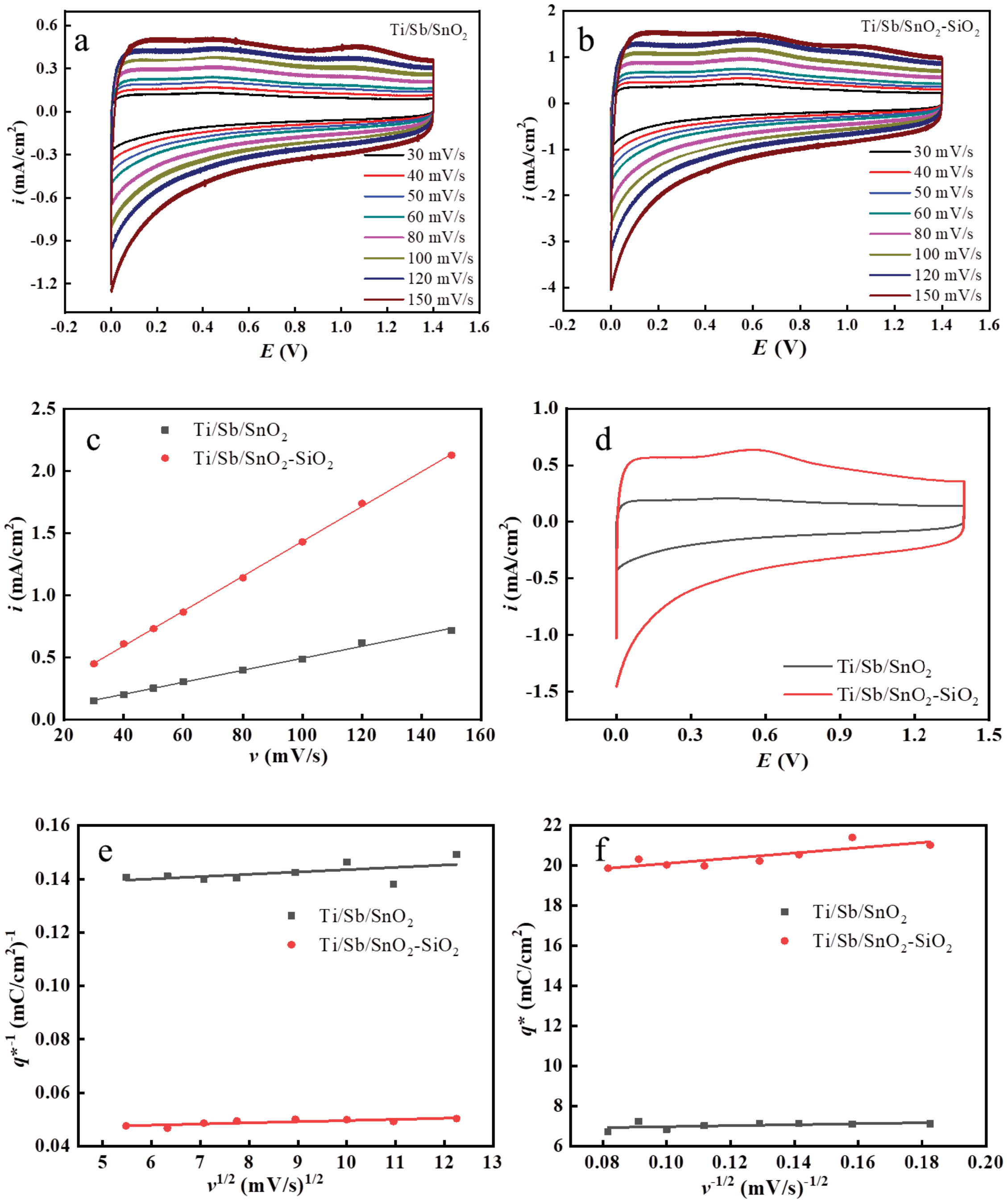

Fig. 5. CV curves of (a) Ti/Sb/SnO_2 and (b) Ti/Sb/SnO_2-SiO_2 at different scan rates, (c) evolution of the current density at 1 V vs. the sweep rate, (d) CV curves of the two electrodes at 50 mV/s; data for (e) Ti/Sb/SnO_2 and (f) Ti/Sb/SnO_2-SiO_2 were obtained from the cyclic voltammograms between 0 and 1.4 V at various scan rates.

after adding SiO_2 nanoparticles, indicating that the addition of SiO_2 nanoparticles speeds up the electrochemical reaction. In addition, lower R_f and higher C_f mean that more OH may be produced on the electrode surface [40,41], indicating that the addition of SiO_2 nanoparticles plays an important role in improving the electrocatalytic oxidation performance of the electrode, which is conducive to the oxidative decomposition of organic pollutants.

Table 2
Voltametric charge and porosity of the two electrodes

Electrode	q_T* (mC/cm²)	q_o* (mC/cm²)	q_i* (mC/cm²)	p
Ti/Sb/SnO_2	7.42	6.73	0.69	0.09
Ti/Sb/SnO_2-SiO_2	22.08	18.80	3.28	0.15

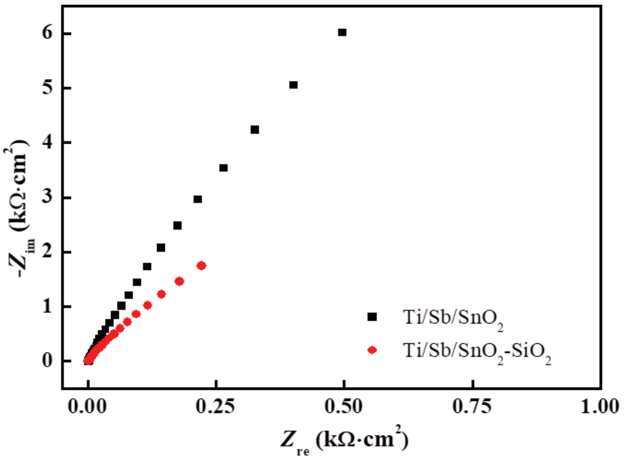

Fig. 6. Electrochemical impedance spectroscopy of two electrodes.

3.3. Electrocatalytic oxidation of organic pollutants

Fig. 8a shows the degradation efficiency of AR 18 as a function of electrocatalytic oxidation time. The results show that the degradation efficiency of AR 18 is significant in the first 60 min and then gradually slows down. After 120 min of electrocatalytic oxidation, the AR 18 degradation efficiency of Ti/Sb/SnO_2-SiO_2 is 99.93% and that of Ti/Sb/SnO_2 is 95.77%. Fig. 8b shows the first-order kinetic degradation process of AR 18, which can be represented by $\ln(c_0/c_t) = k_1t$ (where c_0 is the initial concentration of electrolyte, mg/L; c_t is the concentration of electrolyte at t min, mg/L; t is the time, min, and k_1 is the rate constant, min^{-1}). The k_1 of the Ti/Sb/SnO_2-SiO_2 electrode is greater than that of the Ti/Sb/SnO_2 electrode, indicating that the addition of SiO_2 nanoparticles makes the electrode have a higher degradation rate. The AR 18 is obviously degraded on each electrode, but the degradation efficiency of the Ti/Sb/SnO_2-SiO_2 electrode system is higher.

Meanwhile, the chemical oxygen demand removal rate in the electrocatalytic oxidation process was measured, as shown in Fig. 8c. The removal rate of COD on Ti/Sb/SnO_2-SiO_2 electrodes is continuously higher than Ti/Sb/SnO_2 electrodes. After 120 min of electrocatalytic oxidation, the COD removal rate of Ti/Sb/SnO_2 is 63.9%, while the COD removal rate of Ti/Sb/SnO_2-SiO_2 reaches 81.78%. Fig. 8d displays the first-order kinetic removal process of COD, which can be represented by $\ln(COD_0/COD_t) = k_2t$ (k_2 is the rate constant, min^{-1}). The k_2 of the Ti/Sb/SnO_2-SiO_2 electrode is greater than that of the Ti/Sb/SnO_2 electrode. However, for the same degradation time, the COD removal rate is lower than the AR 18 degradation efficiency, which may mean that the AR 18 is converted into other small molecular organic intermediates before being completely oxidized to CO_2 and H_2O [41,42].

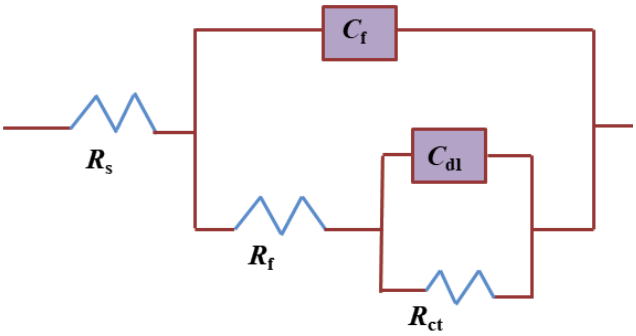

Fig. 7. Equivalent circuit of electrochemical impedance spectroscopy fitting.

The above experiment shows that the AR 18 gradually decomposes during the electrocatalytic oxidation process. In order to further verify the presence of small-molecule organics in the decomposition process of AR 18, the three-dimensional fluorescence spectrum of the organics in the electrolyte with the electrocatalytic oxidation time was measured, and the type of organic matter was determined according to the range of excitation wavelength and emission wavelength. Fig. 9 shows the three-dimensional fluorescence spectrum of the organics in the simulated liquid before electrocatalytic oxidation, which shows that there are no small-molecule organics. Figs. 10 and 11, respectively, show the three-dimensional fluorescence spectra of the changes in the concentration of organic matter in the electrolyte with the electrocatalytic oxidation time when the Ti/Sb/SnO_2 and Ti/Sb/SnO_2-SiO_2 electrodes undergo electrocatalytic oxidation. As can be seen, as the electrocatalytic oxidation process progresses, the AR 18 is gradually decomposed and small organic compounds are formed. Ex/Em is a fulvic-acid-like substance in the range of 220–250/400–500 nm, and Ex/Em is a polycarboxylate humic acid substance in the range of 300–400/400–500 nm [43,44]. The concentration of these small molecule organics first increases over time. With the further extension of the electrocatalytic oxidation time, these small molecular organics are gradually oxidized and their fluorescence intensities gradually weaken. However, comparing the fluorescence intensity changes of the organic matter in Figs. 10 and 11, it can be clearly seen that the small molecular organics in the Ti/Sb/SnO_2-SiO_2 electrode system are oxidized faster than those in the Ti/Sb/SnO_2 electrode system, and the fluorescence intensities of the small molecular organics has become very low after 2 h of electrocatalytic oxidation in the system using the Ti/Sb/SnO_2-SiO_2 electrode.

Table 3
EIS fitting analysis results of the two electrodes

Electrode	R_s (Ω/cm²)	C_f (mF/cm²)	R_f (Ω/cm²)	C_{dl} (mF/cm²)	R_{ct} (kΩ/cm²)
Ti/Sb/SnO_2	1.874	0.968	9.417	0.768	39.85
Ti/Sb/SnO_2-SiO_2	1.442	2.513	2.685	4.762	9.15

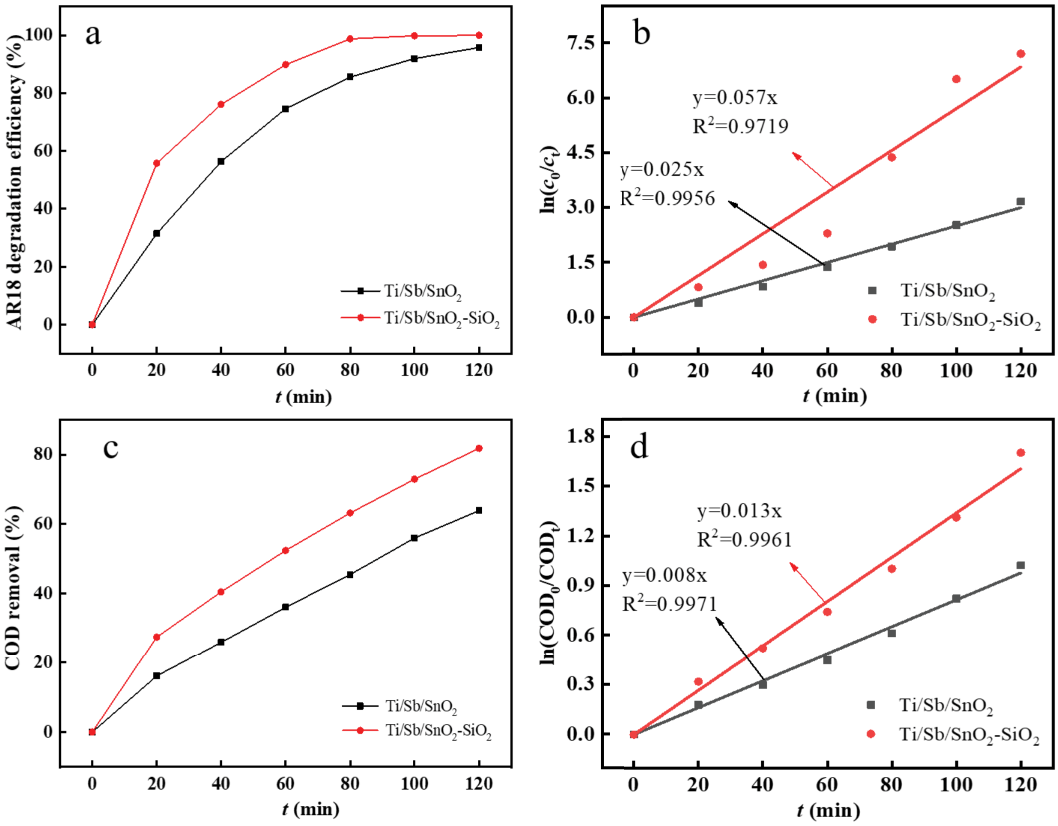

Fig. 8. (a) AR 18 removal efficiency and kinetic fitting of different electrodes and (b) COD removal efficiency and kinetic fitting of different electrodes.

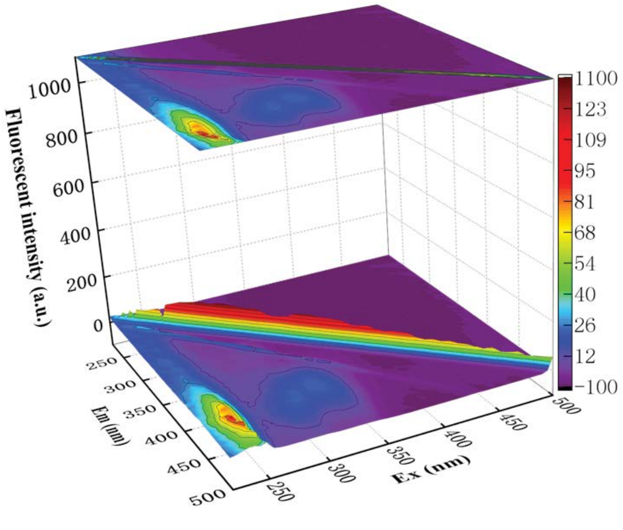

Fig. 9. Three-dimensional fluorescence spectrum of AR 18 before electrocatalytic oxidation.

In the electrocatalytic oxidation process, the degradation efficiency of organic pollutants is closely related to the generation rate and intensity of active oxygen. OH plays an important role in the electrocatalytic oxidation process due to its high redox potential. Therefore, the electrochemical activity of the electrode can be evaluated by measuring the concentration of·OH produced during the electrocatalytic oxidation process. Fig. 12 shows the intensity of OH in the solution before electrocatalytic oxidation. Figs. 13 and 14 show the intensity of •OH produced in the $Ti/Sb/SnO_2$ and $Ti/Sb/SnO_2$-SiO_2 electrode systems, respectively, as a function of electrocatalytic oxidation time. The ability to generate hydroxyl can be compared by considering the fluorescence intensity in Figs. 12–14. It can be seen from Figs. 12–14 that the fluorescence intensity increases with the increase of the reaction time. This indicates that the fluorescence intensity of •OH increases continuously with the progress of electrocatalytic oxidation. The production capacity of •OH on the $Ti/Sb/SnO_2$-SiO_2 electrode is obviously stronger than that on the $Ti/Sb/SnO_2$ electrode, showing that the $Ti/Sb/SnO_2$-SiO_2 electrode with SiO_2 nanoparticles can generate more •OH, which can provide greater electrochemical activity for the electrode, thereby facilitating the electrocatalytic oxidation of organic matter [33,41].

3.4. Current efficiency and energy consumption assessment

The generation capacity of OH affected the current efficiency in the electrocatalytic oxidation process, so the current efficiency was monitored during the process. The instantaneous current efficiency (ICE) of the two electrodes in the degradation process is shown in Fig. 15a, which can be calculated by Eq. (7).

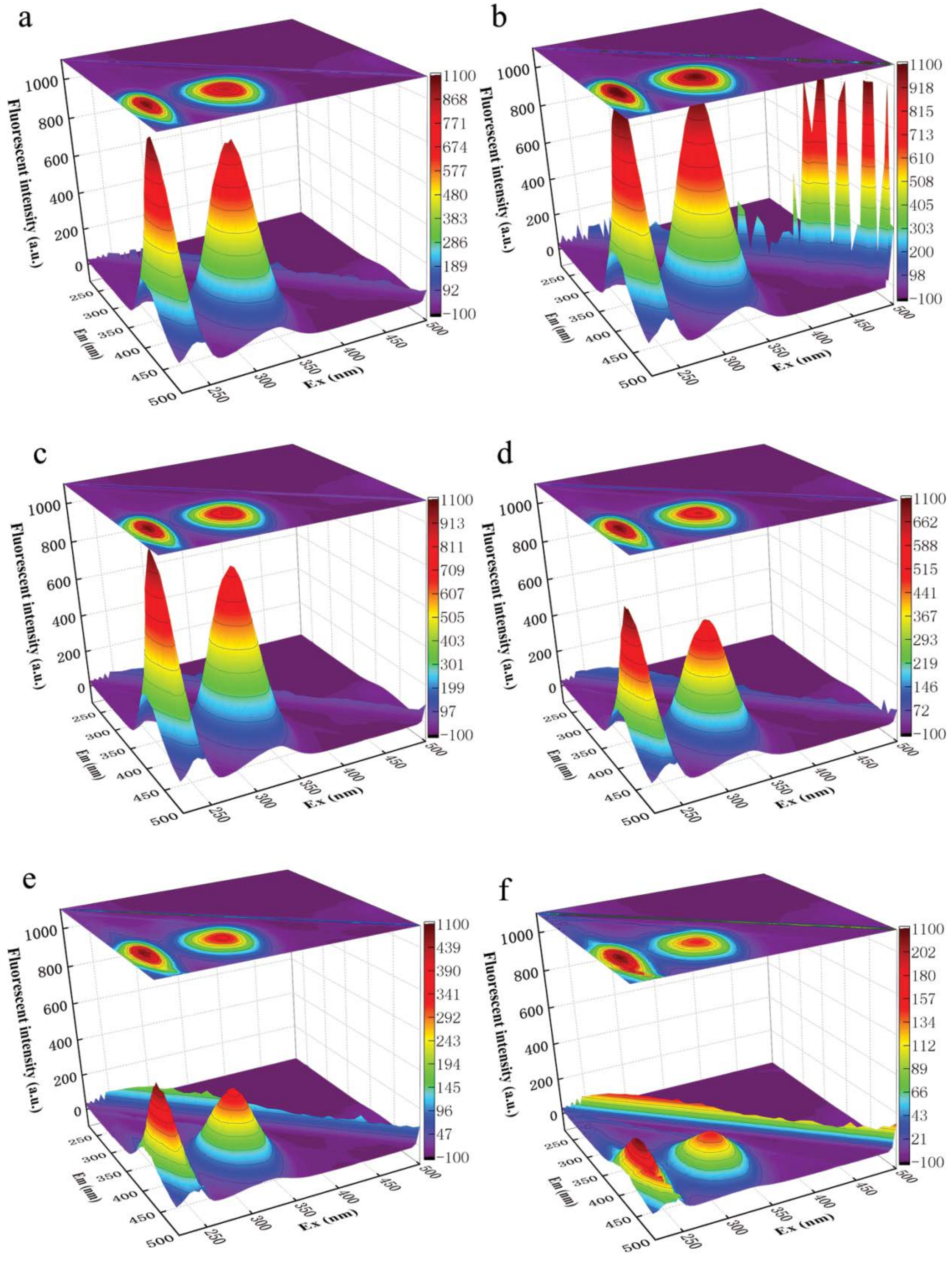

Fig. 10. Three-dimensional fluorescence spectrum of the organic matter concentration in the electrolyte with time during the electrocatalytic oxidation of the Ti/Sb/SnO_2 electrode: (a) 20 min, (b) 40 min, (c) 60 min, (d) 80 min, (e) 100 min, and (f) 120 min.

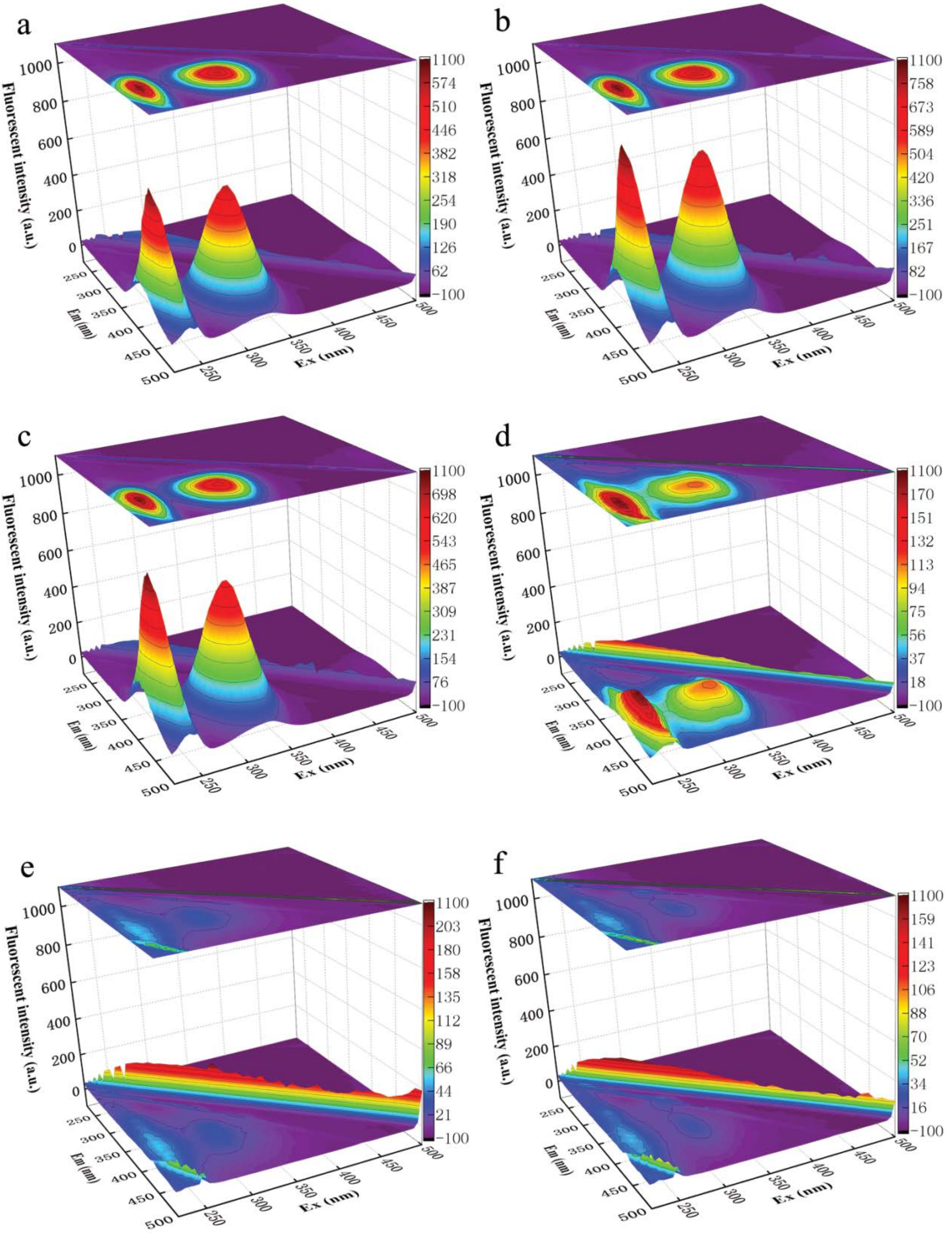

Fig. 11. Three-dimensional fluorescence spectrum of the organic matter concentration in the electrolyte with time during the electrocatalytic oxidation of the Ti/Sb/SnO_2-SiO_2 electrode: (a) 20 min, (b) 40 min, (c) 60 min, (d) 80 min, (e) 100 min, and (f) 120 min.

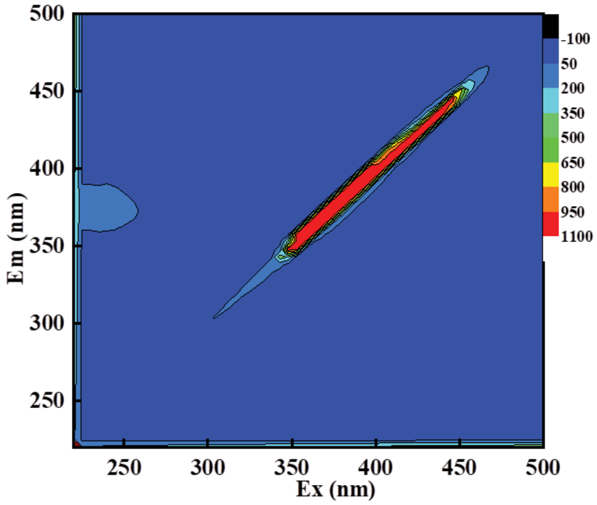

Fig. 12. Fluorescence intensity of OH in the electrolyte before electrocatalytic oxidation.

$$\text{ICE} = \frac{\Delta\text{COD}}{3{,}600 \times 8 \times I \times t} FS_V \times 100\% \quad (7)$$

where ΔCOD is the change value of COD (mg/L); I is the current (A), t is the time (h), S_V is the volume (L); F is the Faraday constant (96,487 C/mol).

After 20 min, the ICE value of Ti/Sb/SnO_2-SiO_2 electrode is 37.29%, which is 1.45 times more than Ti/Sb/SnO_2 electrode. The current efficiency decreases with time, which may be due to a small amount of impurities adsorbed on the surface of the electrodes during the electrolysis process, thus affecting the charge transfer. Compared with the Ti/Sb/SnO_2 electrode, the Ti/Sb/SnO_2-SiO_2 electrode has a higher current efficiency during the process.

In order to evaluate the energy consumption (EC) for degradation of AR 18 in the electrocatalytic oxidation process, the cell voltage of this process was recorded. According to Eq. (8) [45], the energy consumption (EC, kWh/(gCOD)) in the electrocatalytic oxidation process under constant current can be calculated as:

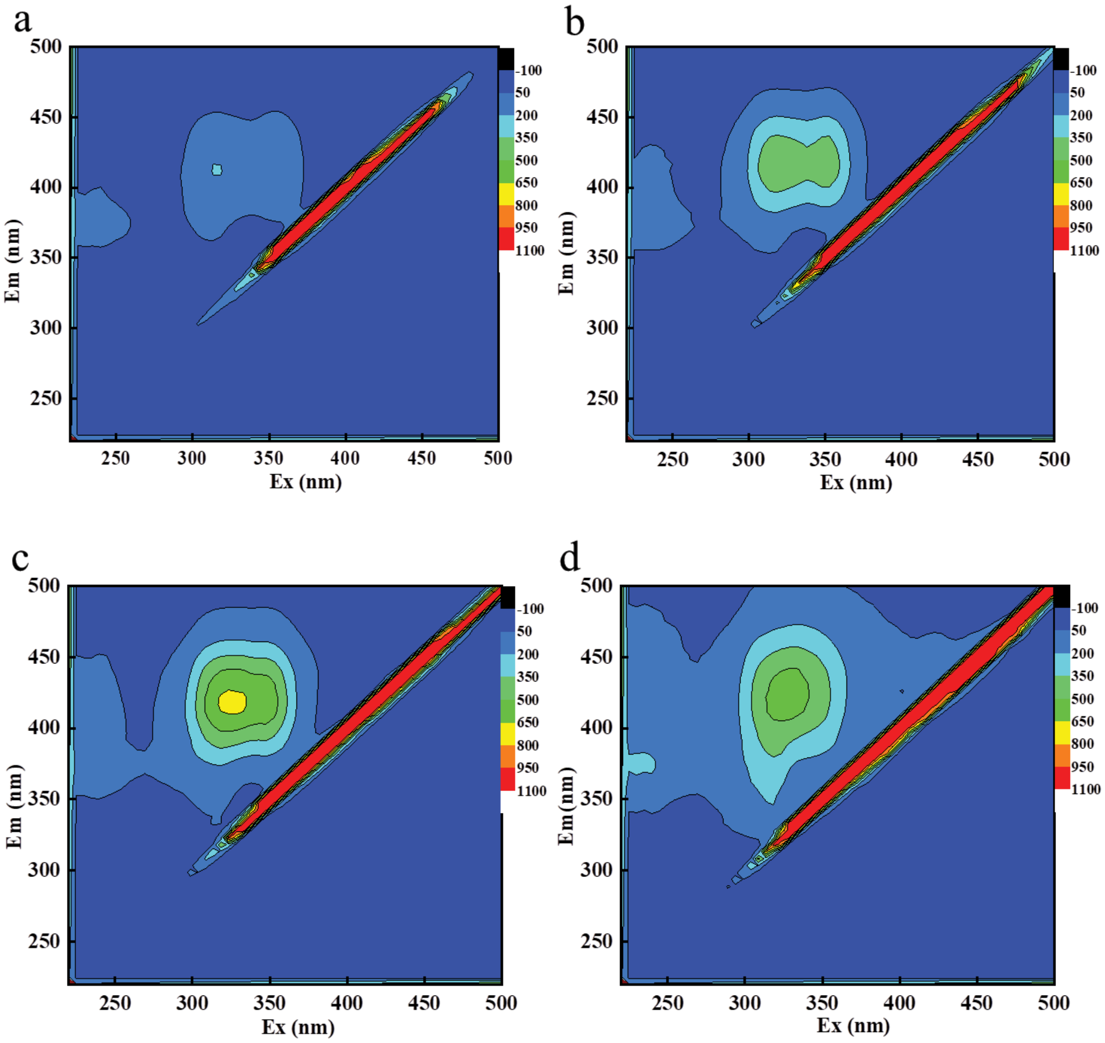

Fig. 13 (Continued)

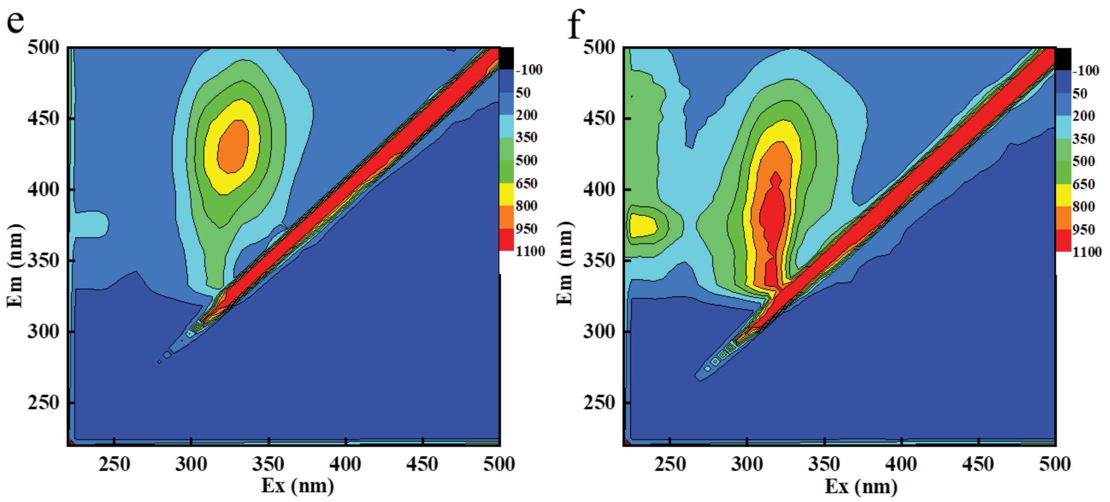

Fig. 13. Fluorescence intensity change of the electrolyte OH with the electrocatalytic oxidation time during the electrocatalytic oxidation of the Ti/Sb/SnO_2 electrode: (a) 20 min, (b) 40 min, (c) 60 min, (d) 80 min, (e) 100 min, and (f) 120 min.

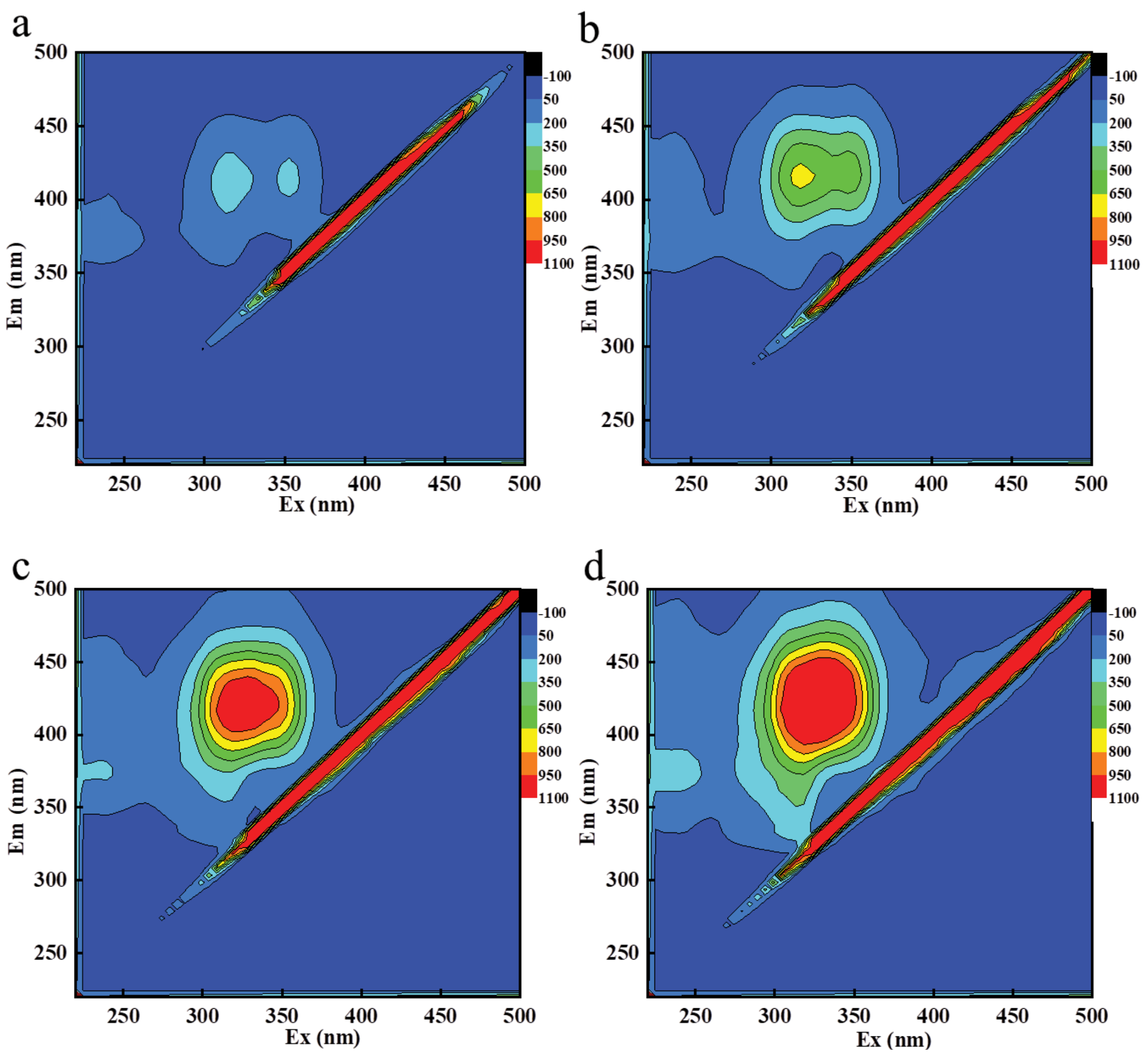

Fig. 14 (Continued)

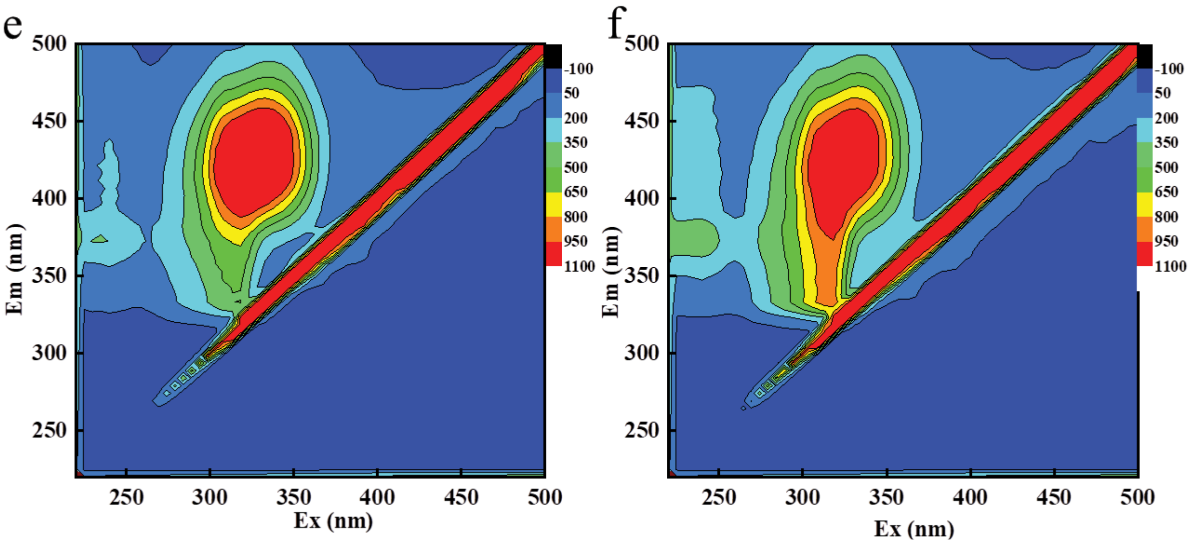

Fig. 14. Fluorescence intensity change of the electrolyte OH with the electrocatalytic oxidation time during the electrocatalytic oxidation of the $Ti/Sb/SnO_2$-SiO_2 electrode: (a) 20 min, (b) 40 min, (c) 60 min, (d) 80 min, (e) 100 min, and (f) 120 min.

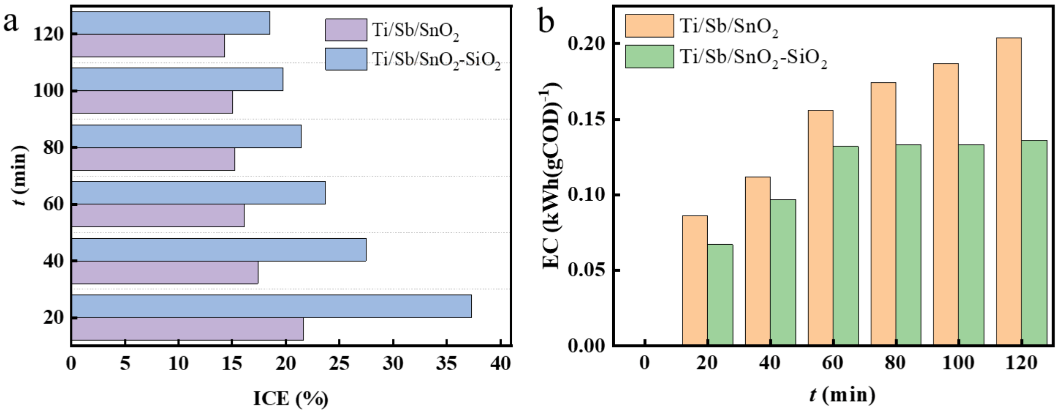

Fig. 15. (a) ICE and (b) EC of the two electrodes in the electrolysis process, respectively.

$$\mathrm{EC}=\frac{UIt}{S_V\Delta\mathrm{COD}} \tag{8}$$

where U is the cell voltage (V).

Fig. 15b analyses the EC of the $Ti/Sb/SnO_2$ and $Ti/Sb/SnO_2$-SiO_2 electrodes during electrocatalytic oxidation. As can be seen from Fig. 15b, the EC of the $Ti/Sb/SnO_2$-SiO_2 electrode gradually stabilized after 1 h of electrocatalytic oxidation. When the electrocatalytic oxidation is carried out for 2 h, the EC of the $Ti/Sb/SnO_2$ electrode is 1.5 times that of the $Ti/Sb/SnO_2$-SiO_2 electrode, indicating adding SiO_2 nanoparticles can significantly reduce the energy consumption in the electrocatalytic oxidation process, improving the stability of the electrode [46].

4. Conclusion

In this work, a novel SiO_2 nano-composite $Ti/Sb/SnO_2$-SiO_2 anode was successfully prepared. For the $Ti/Sb/SnO_2$ electrode added with SiO_2 nanoparticles, since the SiO_2 nanoparticles act as a physical barrier during the thermal decomposition of the coating, the SnO_2 grains could not contact smoothly and formed long-range continuous crystals. This results in finer grains and denser coatings. The addition of SiO_2 nanoparticles increased the oxygen vacancies in the coating and raised the content of active oxygen. The $Ti/Sb/SnO_2$-SiO_2 electrode had a higher oxygen evolution potential, more active sites and volt-ampere charges, which effectively inhibited the side reactions of oxygen evolution and enhanced the catalytic performance of the electrode. After adding SiO_2 nanoparticles, the AR 18 and the COD maximum degradation efficiency of $Ti/Sb/SnO_2$-SiO_2 electrode can reach up 99.93% and 81.78% after 120 min of degradation, respectively. The degradation process of AR 18 conformed to the first-order kinetic reaction. In addition, the OH generation ability of $Ti/Sb/SnO_2$-SiO_2 electrode enhanced, which can effectively improve the current efficiency and reduce the energy consumption, thereby enhancing the stability of the $Ti/Sb/SnO_2$-SiO_2 electrode.

Acknowledgements

This work was financially supported by Natural Science Foundation of Shanghai (Grant Nos. 20ZR1421500) and Science and Technology Commission of Shanghai Municipality (19DZ2271100).

References

[1] Q. Wang, L.P. Liang, F.F. Xi, G.L. Tian, Q.L. Mao, X. Meng, Adsorption of Azo Dye Acid Red 73 onto rice wine lees: adsorption kinetics and isotherms, Adv. Mater. Sci. Eng., 2020 (2020) 3469579, doi: 10.1155/2020/3469579.

[2] N. Mirzaei, H.R. Ghaffari, K. Sharafi, A. Velayati, G. Hoseindoost, S. Rezaei, A.H. Mahvi, A. Azari, K. Dindarloo, Modified natural zeolite using ammonium quaternary based material for Acid red 18 removal from aqueous solution, J. Environ. Chem. Eng., 5 (2017) 3151–3160.

[3] A. Azizi, M.R. Alavi Moghaddam, R. Maknoon, E. Kowsari, Investigation of enhanced Fenton process (EFP) in color and COD removal of wastewater containing Acid Red 18 by response surface methodology: evaluation of EFP as post treatment, Desal. Water Treat., 57 (2015) 14083–14092.

[4] M. Malakootian, H. Mahdizadeh, M. Khavari, A. Nasiri, M.A. Gharaghani, M. Khatami, E. Sahle-Demessie, R.S. Varma, Efficiency of novel Fe/charcoal/ultrasonic micro-electrolysis strategy in the removal of Acid Red 18 from aqueous solutions, J. Environ. Chem. Eng., 8 (2019) 103553, doi: 10.1016/j.jece.2019.103553.

[5] S.C. Deogaonkar, P. Wakode, K.P. Rawat, Electron beam irradiation post treatment for degradation of non biodegradable contaminants in textile wastewater, Radiat. Phys. Chem., 165 (2019) 108377, doi: 10.1016/j.radphyschem.2019.108377.

[6] J.M.P. Ramos, N.M. Pereira-Queiroz, D.H.S. Santos, J.R. Nascimento, C.M. de Carvalho, J. Tonholo, C.L.P.S. Zanta, Printing ink effluent remediation: a comparison between electrochemical and Fenton treatments, J. Water Process Eng., 31 (2019) 100803, doi: 10.1016/j.jwpe.2019.100803.

[7] M. Reza, H. Mahdi, G. Amin, Using of TiO_2/Ag_2O nanocomposite in degradation of Acid Red 18 Dye in photoreactor by Taguchi experimental design, Russ. J. Phys. Chem. A, 93 (2019) 1133–1142.

[8] S. Zahorulko, O. Shmychkova, T. Luk'yanenko, L. Dmitrikova, A. Velichenko, The comparative study of electrocatalytic activity of various anode materials in respect to the oxidation of nitroanilines, Mater. Today Proc., 6 (2019) 242–249.

[9] C. Geng, Z.J. Liang, F.Y. Cui, Z.W. Zhao, C. Yuan, J.Y. Du, C. Wang, Energy-saving photo-degradation of three fluoroquinolone antibiotics under VUV/UV irradiation: kinetics, mechanism, and antibacterial activity reduction, Chem. Eng. J., 383 (2020) 123145, doi: 10.1016/j.cej.2019.123145.

[10] M. Baca, M. Aleksandrzak, E. Mijowska, R.J. Kaleńczuk, B. Zielińska, Core/shell structure of mesoporous carbon spheres and $g\text{-}C_3N_4$ for Acid Red 18 decolorization, Catalysts, 9 (2019) 1007, doi: 10.3390/catal9121007.

[11] B.M. Souza-Chaves, M. Dezotti, C.D. Vecitis, Synergism of ozonation and electrochemical filtration during advanced organic oxidation, J. Hazard. Mater., 382 (2020) 121085, doi: 10.1016/j.jhazmat.2019.121085.

[12] D. Zhi, J.B. Wang, Y.Y. Zhou, Z.R. Luo, Y.Q. Sun, Z.H. Wan, L. Luo, D.C.W. Tsang, D.D. Dionysiou, Development of ozonation and reactive electrochemical membrane coupled process: enhanced tetracycline mineralization and toxicity reduction, Chem. Eng. J., 383 (2020) 123149, doi: 10.1016/j.cej.2019.123149.

[13] A.M. Chávez, R.R. Solís, F.J. Beltrán, Magnetic graphene TiO_2-based photocatalyst for the removal of pollutants of emerging concern in water by simulated sunlight aided photocatalytic ozonation, Appl. Catal., B, 262 (2020) 118275, doi: 10.1016/j.apcatb.2019.118275.

[14] A. Ansari, D. Nematollahi, Convergent paired electrocatalytic degradation of *p*-dinitrobenzene by $Ti/SnO_2\text{-}Sb/\beta\text{-}PbO_2$ anode. A new insight into the electrochemical degradation mechanism, Appl. Catal., B, 261 (2020) 118226, doi: 10.1016/j.apcatb.2019.118226.

[15] Z. Zhang, C. Teng, K. Zhou, C. Peng, W. Chen, Degradation characteristics of dissolved organic matter in nanofiltration concentrated landfill leachate during electrocatalytic oxidation, Chemosphere, 255 (2020) 127055, doi: 10.1016/j.chemosphere.2020.127055.

[16] J.X. Feng, J.X. Sun, X.S. Liu, J.Z. Zhu, S.H. Tian, R. Wu, Y. Xiong, Coupling effect of piezomaterial and DSA catalyst for degradation of metronidazole: finding of induction electrocatalysis from remnant piezoelectric filed, J. Catal., 381 (2020) 530–539.

[17] A.Q. Chen, S.J. Xia, Z.G. Ji, H.W. Lu, Insights into the origin of super-high oxygen evolution potential of Cu doped SnO_2 anodes: a theoretical study, Appl. Surf. Sci., 471 (2019) 149–153.

[18] A.Q. Chen, S.V. Nair, B. Miljkovic, H.E. Ruda, Z.G. Ji, A DFT computational study of the mechanism of super-high oxygen evolution potential of W doped SnO_2 anodes, Electroanal. Chem., 855 (2019) 113499, doi: 10.1016/j.jelechem.2019.113499.

[19] G. de O S Santos, V.M. Vasconcelos, R.S. da Silva, M.A. Rodrigo, K.I.B. Eguiluz, G.R. Salazar-Banda, New laser-based method for the synthesis of stable and active Ti/SnO_2–Sb anodes, Electrochim. Acta, 332 (2020) 135478, doi: 10.1016/j.electacta.2019.135478.

[20] G.S. Szymański, M. Wiśniewski, P. Olejnik, S. Koter, E. Castro, L. Echegoyen, A.P. Terzyk, M.E. Plonska-Brzezinska, Correlation between the catalytic and electrocatalytic properties of nitrogen-doped carbon nanoonions and the polarity of the carbon surface: experimental and theoretical investigations, Carbon, 151 (2019) 120–129.

[21] T.G. Duan, L. Ma, Y. Chen, X. Ma, J. Hou, C.G. Lin, M.X. Sun, Morphology-dependent activities of TiO_2-NTs@Sb-SnO_2 electrodes for efficient electrocatalytic methyl orange decolorization, J. Solid State Electrochem., 22 (2018) 1871–1879.

[22] F.P. Hu, X.W. Cui, W.X. Chen, Pulse electro-codeposition of Ti/SnO_2–Sb_2O_4–CNT electrode for phenol oxidation, Electrochem. Solid-State Lett., 13 (2010), doi: 10.1149/1.3457858.

[23] H. Pourzamani, Y. Hajizadeh, N. Mengelizadeh, Application of three-dimensional electro-Fenton process using MWCNTs-Fe_3O_4 nanocomposite for removal of diclofenac, Process Saf. Environ. Prot., 119 (2018) 271–284.

[24] L. Mais, M. Mascia, S. Palmas, A. Vacca, Photoelectrochemical oxidation of phenol with nanostructured TiO_2-PANI electrodes under solar light irradiation, Sep. Purif. Technol., 208 (2019) 153–159.

[25] F. Xu, L. Chang, X. Duan, W. Bai, X. Sui, X. Zhao, A novel layer-by-layer CNT/PbO_2 anode for high-efficiency removal of PCP-Na through combining adsorption/electrosorption and electrocatalysis, Electrochim. Acta, 300 (2019) 53–66.

[26] L. Gan, Y. Wu, H. Song, C. Lu, S. Zhang, A. Li, Self-doped TiO_2 nanotube arrays for electrochemical mineralization of phenols, Chemosphere, 226 (2019) 329–339.

[27] A. Anagnostopoulos, A. Palacios, M.H. Navarro, S. Fereres, Y.L. Ding, Effect of SiO_2 nanoparticle addition on the wetting and rheological properties of solar salt, Sol. Energy Mater. Sol. Cells, 210 (2020) 110483.

[28] S.R. Karnati, P. Agbo, L.F. Zhang, Applications of silica nanoparticles in glass/carbon fiber-reinforced epoxy nanocomposite, Compos. Commun., 17 (2020) 32–41.

[29] T.T. Ren, G.W. Tang, B. Yuan, Y. Yang, Z.S. Yan, L.R. Ma, X. Huang, Hexadecyltrimethoxysilane-modified SiO_2 nanoparticle-coated halloysite nanotubes embedded in silicone-acrylic polymer films as durable fluorine-free superhydrophobic coatings, ACS Appl. Nano Mater., 3 (2020) 5807–5815.

[30] Y. Song, J. Liu, F. Ge, X. Huang, Y. Zhang, H. Ge, X. Meng, Y. Zhao, Influence of Nd-doping on the degradation performance of Ti/Sb-SnO_2 electrode, J. Environ. Chem. Eng., 9 (2021) 105409, doi: 10.1016/j.jece.2021.105409.

[31] Q. Bi, W. Guan, Y. Gao, Y. Cui, S. Ma, J. Xue, Study of the mechanisms underlying the effects of composite intermediate layers on the performance of Ti/SnO_2-Sb-La electrodes, Electrochim. Acta, 306 (2019) 667–679.

[32] Y. Zhang, P. He, L. Jia, C. Li, H. Liu, S. Wang, S. Zhou, F. Dong, Ti/PbO_2-Sm_2O_3 composite based electrode for highly efficient electrocatalytic degradation of alizarin yellow R, J. Colloid Interface Sci., 533 (2019) 750–761.

[33] L. Zhang, L. Xu, J. He, J. Zhang, Preparation of Ti/SnO_2-Sb electrodes modified by carbon nanotube for anodic oxidation of dye wastewater and combination with nanofiltration, Electrochim. Acta, 117 (2014) 192–201.

[34] Y. Sun, S. Cheng, Z. Mao, Z. Lin, X. Ren, Z. Yu, High electrochemical activity of a Ti/SnO_2–Sb electrode electrodeposited using deep eutectic solvent, Chemosphere, 239 (2020) 124715, doi: 10.1016/j.chemosphere.2019.124715.

[35] W.Y. Wang, X.Y. Duan, X.Y. Sui, Q. Wang, F. Xu, L.M. Chang, Surface characterization and electrochemical properties of PbO_2/SnO_2 composite anodes for electrocatalytic oxidation of *m*-nitrophenol, Electrochim. Acta, 335 (2020) 135649, doi: 10.1016/j.electacta.2020.135649.

[36] E.C.P.E. Rodrigues, P. Olivi, Preparation and characterization of Sb-doped SnO_2 films with controlled stoichiometry from polymeric precursors, J. Phys. Chem. Solids, 64 (2003) 1105–1112.

[37] L. Xu, Y. Yi, G.R. Liang, W. Zhang, Antimony doped tin oxide nanoparticles deposited onto Nb−TiO_2 nanotubes for electrochemical degradation of bio-refractory pollutions, Electroanalysis: An Int. J. Devoted Electroanal. Sens. Bioelectronic Devices, 32 (2020) 1370–1378.

[38] Y. Wang, H.Y. Duan, Z.H. Pei, L. Xu, Hydrothermal synthesis of 3D hierarchically flower-like structure Ti/SnO_2-Sb electrode with long service life and high electrocatalytic performance, Electroanal. Chem., 855 (2019) 113635, doi: 10.1016/j.jelechem.2019.113635.

[39] T. Duan, Y. Chen, Q. Wen, Y. Duan, Different mechanisms and electrocatalytic activities of Ce ion or CeO_2 modified Ti/Sb–SnO_2 electrodes fabricated by one-step pulse electro-codeposition, RSC Adv., 5 (2015) 19601–19612.

[40] C.B. Tang, Y.X. Lu, F. Wang, H. Niu, L.H. Yu, J.Q. Xue, Influence of a MnO_2-WC interlayer on the stability and electrocatalytic activity of titanium-based PbO_2 anodes, Electrochim. Acta, 331 (2020) 135381, doi: 10.1016/j.electacta.2019.135381.

[41] B. Zhao, H.B. Yu, Y. Lu, J. Qu, S.Y. Zhu, M.X. Huo, Polyethylene glycol assisted synthesis of a praseodymium-doped PbO_2 electrode and its enhanced electrocatalytic oxidation performance, J. Taiwan Inst. Chem. Eng., 100 (2019) 144–150.

[42] Y. Yao, G. Teng, Y. Yang, C. Huang, B. Liu, L. Guo, Electrochemical oxidation of acetamiprid using Yb-doped PbO_2 electrodes: electrode characterization, influencing factors and degradation pathways, Sep. Purif. Technol., 211 (2019) 456–466.

[43] S.S. Yang, W.Q. Guo, Y.D. Chen, Q.L. Wu, H.C. Luo, S.M. Peng, H.S. Zheng, X.C. Feng, X. Zhou, N.Q. Ren, Economical evaluation of sludge reduction and characterization of effluent organic matter in an alternating aeration activated sludge system combining ozone/ultrasound pretreatment, Bioresour. Technol., 177 (2015) 194–203.

[44] T.-M. Hwang, S.-H. Nam, J. Lee, J.-W. Koo, E. Kim, M. Kwon, Hydroxyl radical scavenging factor measurement using a fluorescence excitation-emission matrix and parallel factor analysis in ultraviolet advanced oxidation processes, Chemosphere, 259 (2020) 127396, doi: 10.1016/j.chemosphere.2020.127396.

[45] D. Lim, Y. Kim, D. Nam, S. Hwang, S.E. Shim, S.-H. Baeck, Influence of the Sb content in Ti/SnO_2-Sb electrodes on the electrocatalytic behaviour for the degradation of organic matter, J. Cleaner Prod., 197 (2018) 1268–1274.

[46] Y. Zhang, P. He, L. Jia, T. Zhang, H. Liu, S. Wang, C. Li, F. Dong, S. Zhou, Dimensionally stable Ti/SnO_2-RuO_2 composite electrode based highly efficient electrocatalytic degradation of industrial gallic acid effluent, Chemosphere, 224 (2019) 707–715.